Optimal Diffractive Focusing of Matter and Light Waves

Maxim A. Efremov[®], ^{1,2,*} Felix Hufnagel, Hugo Larocque[®], Wolfgang P. Schleich[®], ^{2,5} and Ebrahim Karimi[®], 6 ¹German Aerospace Center (DLR), Institute of Quantum Technologies, 89081 Ulm, Germany 2 Institut für Quantenphysik and Center for Integrated Quantum Science and Technology (IQST), Universität Ulm, 89081 Ulm, Germany ³Nexus for Quantum Technologies, University of Ottawa, K1N 5N6 Ottawa, Ontario, Canada ⁴Research Laboratory of Electronics, Massachusetts Institute of Technology, Cambridge, Massachusetts 02139, USA ⁵Hagler Institute for Advanced Study at Texas A&M University, Texas A&M AgriLife Research, Institute for Quantum Science and Engineering (IQSE), and Department of Physics and Astronomy, Texas A&M University, College Station, Texas 77843-4242, USA ⁶Institute for Quantum Studies, Chapman University, Orange, California 92866, USA

(Received 11 August 2024; revised 4 June 2025; accepted 5 August 2025; published 12 September 2025)

Following the familiar analogy between the optical paraxial wave equation and the Schrödinger equation, we derive the optimal, real-valued wave function for focusing in one- and two-space dimensions without the use of any phase component. We compare and contrast the focusing parameters of the optimal waves with those of other diffractive focusing approaches, such as Fresnel zones. Moreover, we experimentally demonstrate these focusing properties on optical beams using both reflective and transmissive liquid crystal devices. Our results provide an alternative direction for focusing waves where phase elements are challenging to implement, such as for x-rays, THz radiation, and electron beams.

DOI: 10.1103/h6yy-vvmf

Introduction—Fresnel zone plates [1] are optical elements that focus an incident beam due to binary variations in its amplitude and phase. They offer precise control over diffractive propagation and enable beam focusing in systems where traditional lensing elements are not immediately available. In this Letter, we address the fundamental question of whether any other approach to wave shaping, based entirely on the modulation of a wave amplitude, can surpass the limit set by a Fresnel zone plate. We show for the case of matter, optical, and any other waves subjected to paraxial propagation, that the technique of amplitude modulation (diffractive focusing) has (i) a fundamental limit, dictated by their wave nature, and (ii) does yield more efficient focusing than Fresnel lenses by a factor fundamentally constrained to $\pi^2/4$. Moreover, we demonstrate our approach and compare it to Fresnel zone plates by an optical experiment.

A scalar wave, such as a matter wave or an unpolarized electromagnetic field, comprises two components: an amplitude and a phase. The common way to focus an electromagnetic wave is to modulate its phase using a lens by applying a parabolic phase variation in space. This approach forms the pillar of both standardized and emerging imaging systems [2-4], such as lenses implemented

Published by the American Physical Society under the terms of the Creative Commons Attribution 4.0 International license. Further distribution of this work must maintain attribution to the author(s) and the published article's title, journal citation, and DOI.

with metasurfaces [5] or multilevel diffractive phase masks [6]. However, there are waves for which a phase-modulating lens does not exist due to technological limitations in implementing phase-altering components in these systems. For instance, implementing such components for x-rays and matter waves often requires subnanometer manufacturing.

There exist alternative approaches to focusing waves via amplitude modulation in space. For example, blocking part of the wave by a circular aperture or annular rings known as Fresnel zones will focus it to the Arago-Poisson spot [1]. In these examples, the incoming waves are spatially selected without being modified by the materials. These diffractive focusing techniques are crucially determined by a non-Gaussian initial wave function, as well as by the underlying dimensionality of the problem [7-9], and have been employed for surface gravity water waves and plasmonic waves [10,11], as well as for a Bose-Einstein condensate [12].

We emphasize that Fresnel zones provide one approach to focusing the waves by amplitude modulation; one may question whether other approaches, e.g., nonbinary amplitude modulations, provide even better focusing. In this Letter, we obtain the optimal initial wave function for focusing matter waves in one and two dimensions, and compare and contrast the focusing parameters of the optimal two-dimensional wave function to those of the Fresnel zone approach. Because of the same form of the Schrödinger and the paraxial Helmholtz equations, we are able to extend our results to electromagnetic waves. In contrast to Fresnel zone plates producing infinitely many foci with the low efficiency at each focus [13], the optimal

Contact author: maxim.efremov@dlr.de

wave function provides most efficient focusing with a single focus. Finally, we experimentally verify the focusing properties of the two-dimensional pattern at optical wavelengths using a reflective spatial light modulator and a fabricated transmissive liquid crystal device.

Theory of optimal focusing—Our goal is to determine the optimal initial real-valued wave function ψ_0 in two spatial dimensions that maximizes the intensity $|\psi|^2$ of the field on the symmetry axis at a prescribed focusing time. This initial wave function should be normalized and constrained to a finite aperture.

We assume that ψ_0 is radially symmetric, as it provides the best diffractive focusing [8], and write the solution as

$$\psi(\rho, \tau) = 2\pi \int_0^\infty \rho' d\rho' G^{(2)}(\rho, \tau | \rho', 0) \psi_0(\rho') \qquad (1)$$

of the time-dependent two-dimensional Schödinger equation of a free particle in terms of the corresponding Green's function

$$G^{(2)}(\rho, \tau | \rho', 0) = \frac{1}{2\pi i \tau} \exp\left(i\frac{\rho^2 + {\rho'}^2}{2\tau}\right) J_0\left(\frac{\rho \rho'}{\tau}\right) \quad (2)$$

with the Bessel function J_0 of the first kind [14]. Here $\rho \equiv r/R$ and $\tau \equiv \hbar t/(MR^2)$ are the dimensionless radial coordinate and time, respectively, wherein M and R denote the mass of the particle and the radius of the circular aperture. In the case of the two-dimensional paraxial Helmholtz equation, τ is equivalent to the longitudinal distance $z \equiv kR^2\tau$ from the screen, where k denotes the wave number.

We consider only wave functions ψ_0 that are truncated by the aperture $\rho \le 1$ and vanish elsewhere, $\psi_0(\rho \ge 1) = 0$. As a result, for a prescribed focusing time $\tau_{\rm f}$, or focal distance $z_{\rm f} \equiv kR^2\tau_{\rm f}$, the intensity $I[\psi_0]$ along the symmetry axis, $\rho = 0$, takes the form

$$I[\psi_0] = \frac{1}{\tau_f^2} \int_0^1 u du \int_0^1 v dv \cos\left(\frac{u^2 - v^2}{2\tau_f}\right) \psi_0(u) \psi_0(v),$$
(3)

where we have used that ψ_0 is real.

In order to solve the optimization problem, we first construct the Lagrange function

$$\mathcal{L}[\psi_0] \equiv I[\psi_0] - \lambda \left[2\pi \int_0^1 u \mathrm{d}u \, \psi_0^2(u) - 1 \right], \tag{4}$$

where the Lagrange multiplier λ takes into account the normalization condition for ψ_0 , and then perform the variation of $\mathcal{L}[\psi_0]$ with respect to ψ_0 , to arrive at the eigenvalue problem

$$\frac{1}{2\pi\tau_{\rm f}^2} \int_0^1 v \, \mathrm{d}v \, \cos\left(\frac{u^2 - v^2}{2\tau_{\rm f}}\right) \psi_0(v) = \lambda \psi_0(u) \qquad (5)$$

for the optimal wave function ψ_0 corresponding to the eigenvalue λ .

Since Eq. (5) is a linear integral equation with a degenerate kernel, its solution can be found analytically, as shown in Appendix A. Indeed, for a fixed value of τ_f , we obtain the maximum eigenvalue

$$\lambda_{+}(\tau_{\rm f}) = \frac{1}{8\pi\tau_{\rm f}^2} \left[1 + 2\tau_{\rm f} \left| \sin\left(\frac{1}{2\tau_{\rm f}}\right) \right| \right] \tag{6}$$

and the normalized optimal initial wave function

$$\psi_0^{(\text{opt})}(\rho) = N \left[\sqrt{1+a} \cos\left(\frac{\rho^2}{2\tau_f}\right) + \sqrt{1-a} \sin\left(\frac{\rho^2}{2\tau_f}\right) \right]. \tag{7}$$

Here, $a \equiv \cos[1/(2\tau_{\rm f})] \sin[1/(2\tau_{\rm f})]$ and $N \equiv 1/\sqrt{8\pi^2\tau_{\rm f}^2\lambda_+(\tau_{\rm f})}$ are the amplitude parameter and the normalization constant, respectively, with ${\rm sign}(x)$ being the sign function.

the sign function. Substituting $\psi_0^{(\text{opt})}$ given by Eq. (7) into the expression Eq. (3) for the intensity at $\rho=0$, we prove that the intensity, indeed, achieves its maximum value $I_{\max}^{(\text{opt})}(\tau_{\mathrm{f}}) \equiv I[\psi_0^{(\text{opt})}] = \lambda_+(\tau_{\mathrm{f}})$ for any given focusing time τ_{f} , or the dimensionless distance z_{f} from the screen (within the paraxial approximation). In particular, for

$$\tau_{n_0} \equiv \frac{1}{2\pi n_0},\tag{8}$$

where the integer n_0 counts the number of Fresnel zones that fit in the circular aperture $0 \le \rho \le 1$, Eq. (6) yields

$$I_{\text{max}}^{(\text{opt})}(\tau_{n_0}) = \frac{\pi}{2}n_0^2.$$
 (9)

Fresnel zones—Next we compare the maximum focusing intensity, Eq. (9), of the optimal state $\psi_0^{(\text{opt})}$ with the Fresnel zones approach. For this purpose, we consider two different designs.

An amplitude Fresnel zone (AFZ) plate alters the amplitude, while the phase Fresnel zone (PFZ) plate modifies the phase of the incoming wave. In the AFZ, only odd (n=1,3,5,...) annular zones are transparent, whereas even (n=2,4,6,...) zones are opaque, that is absorbing the incoming waves, with n=1 being the innermost zone containing the origin. The AFZ plate is a nonunitary object, i.e., the input intensity is not conserved. In the PFZ, we keep even and odd zones fully transparent; however, the phase in the even zones is shifted by π .

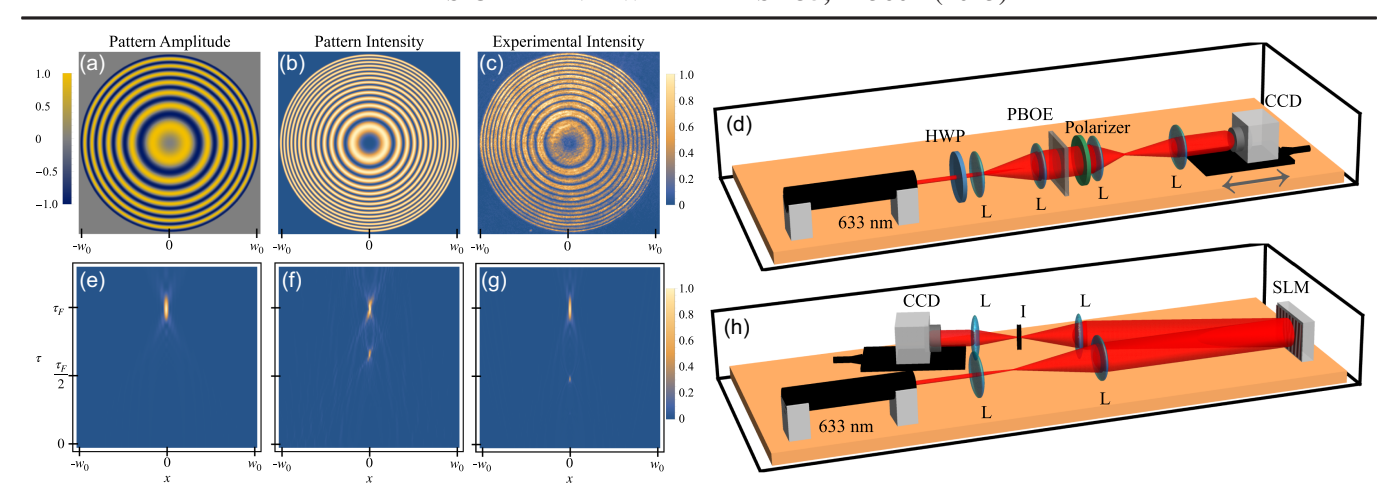


FIG. 1. Implementation of optimal diffractive focusing. We show the theoretical amplitude (a) and intensity (b) of the $n_0=14$ optimal wave together with the measured optical transmission through the fabricated focusing element (c) for the focusing time $\tau_{n_0}=1/(2\pi n_0)$. (d) Experimental apparatus used to generate the optimal state with a PBOE. A linearly polarized 633 nm Gaussian beam passes through a half-wave plate (HWP), which rotates it to the horizontal polarization. The beam is then expanded by a factor of five by two lenses (L) to obtain a relatively flat profile before it goes through the PBOE followed by a polarizer. The latter is then imaged by a 4f-system in order to examine its propagation dynamics by a CCD camera. Numerically simulated (e) and experimentally observed (f) intensity distributions for a cross section of the beam as it propagates from the plane of the device to the focus for the optimal state. Numerical simulation taking into account contributions (g) from both the horizontal (cosine) and vertical (sine) polarization components of the modulated beam. Experimental setup (h) for focusing with Fresnel zone patterns using the SLM. The 633 nm laser source is expanded to cover the SLM. The 4f-lens system then images the SLM onto the CCD camera with an iris (I) placed at the focus to select the first order of diffraction.

For the focusing time τ_{n_0} , we derive in Appendix B the maximal intensities

$$I_{\rm max}^{\rm (AFZ)}(\tau_{n_0}) = \frac{2}{\pi} \begin{cases} n_0(n_0+1), & n_0=1,3,5,\dots \\ n_0^2, & n_0=2,4,6,\dots \end{cases} \eqno(10)$$

and

$$I_{\text{max}}^{(\text{PFZ})}(\tau_{n_0}) = -\frac{4}{\pi}n_0^2 \tag{11}$$

at the symmetry axis $\rho = 0$.

A comparison of Eqs. (9) and (10) reveals that the optimal state $\psi_0^{\text{(opt)}}$ defined by Eq. (7) does give rise to focusing improved by the factor $\pi^2/4$ in the achieved intensity compared to the conventional AFZ method. Moreover, in contrast to AFZ producing many foci with low efficiency [13], the optimal state produces a single spot with the maximal efficiency. These are our central results. They solve a critical problem of finding the optimal realvalued profile, which provides the best focusing without a phase modulation (a lens). Moreover, our results have significant impact for valuable applications in x-ray optics, THz imaging, and electron microscopy. Indeed, for such waves, lenses are either unavailable or difficult to implement due to the challenges of imprinting the parabolic phase profile otherwise required for focusing. Therefore, schemes relying on AFZ become a viable alternative to focus such waves. For these types of matter and light waves, our approach of the optimal diffractive focusing gives an improvement of $\pi^2/4 \approx 2.5$ compared to the existing schemes.

Experiments—Now we demonstrate experimentally optimal diffractive focusing for the two-dimensional case of electromagnetic waves. For this purpose we have fabricated a transmissive, liquid crystal-based Pancharatnam Berry optical element (PBOE) [15], described in Appendix C, which can be operated at many different wavelengths. It generates the optimal state $\psi_0^{(\text{opt})}$ given by Eq. (7). The space-varying amplitude for the focusing time τ_{n_0} defined by Eq. (8) with $n_0=14$ is shown in Fig. 1(a) together with the expected and measured intensities, Figs. 1(b) and 1(c), respectively.

The experimental apparatus used to generate the optimal state is displayed in Fig. 1(d). The PBOE placed between a a half-wave plate (HWP) and a polarizer is illuminated by a 633 nm He-Ne laser with an expanded Gaussian profile. A 4-f lens system is used to image the device on a 1920×1080 pixel CCD camera placed on a translation stage, which allows us to measure the intensity of the modulated beam along its propagation toward the focus. We have obtained this intensity profile in 50 μm steps over 25 mm.

Whereas Fig. 1(e) shows the exact evolution of the beam originating from the optimal state $\psi_0^{(\text{opt})}$ given by Eq. (7), Figs. 1(f) and 1(g) display the experimentally measured and expected intensity along the beam's propagation axis. As further elaborated in the Discussion section, we expect

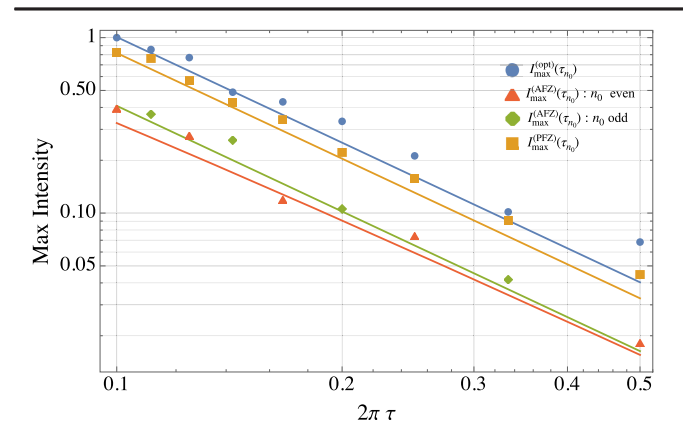


FIG. 2. Comparison of the three methods for two-dimensional diffractive focusing. For a fixed focusing time $\tau_{n_0}=1/(2\pi n_0)$, with $n_0=2,3,\ldots,10$, we display the theoretical optimal maximum intensities, $I_{\rm max}^{\rm (opt)}(\tau_{n_0})$ (blue line), given by Eq. (9), as well as $I_{\rm max}^{\rm (AFZ)}(\tau_{n_0})$ (red and green), and $I_{\rm max}^{\rm (PFZ)}(\tau_{n_0})$ (orange), associated with the Fresnel zone plates, Eqs. (10) and (11). The shift between the blue (dots) and the green (diamond), or the blue and the orange (squares) lines show the improvement of the optimal focusing method compared to AFZ, or PFZ.

imperfections in our optical system to affect the propagation profile.

To compare the propagation of $\psi_0^{(\text{opt})}$ with the ones created by the Fresnel zone plates (Appendix B), we replace our PBOE by a reflective spatial light modulator (SLM), as depicted in Fig. 1(h). We used a Hamamatsu liquid crystal on silicon SLM with 1272×1024 resolution and a pixel size of 12.5 µm. Moreover, we are able to encode both the intensity and the phase of the pattern on the incident beam using an amplitude masking technique [16]. A phase diffraction grating is added to the pattern on the SLM, which produces the desired field in the first order of diffraction. We then select this first order with a 4-f lens system and an iris, thereby allowing us to remove all other diffraction orders while imaging the SLM plane onto our moveable CCD camera. Although SLMs do not reach the spatial resolution of our PBOE, their programmability can more readily streamline experiments comparing various focusing approaches.

In Fig. 2, we display the maximal focusing intensity $I_{\max}(\tau_{n_0})$ for nine different patterns corresponding to focusing times τ_{n_0} , as defined in Eq. (8), with $n_0 = 2, 3, ..., 10$. The results of these experiments involving the optimal wave function as well as both forms of the Fresnel zones are depicted in Fig. 2.

Discussion—The propagation of the beam, shown in Fig. 1(f), features an artificial peak at $\tau = \tau_f/2$ arising from the modulation by our PBOE. Indeed, an imperfect polarization alignment in our generation apparatus leads to contributions from a parasitic beam proportional to $\sin(2\alpha)$, where $\alpha = \alpha(x, y)$ is the relative orientation of

the liquid crystals. This component is not part of the optimal solution presented in this work (Appendix C). Here, α ranges from 0 to $\pi/2$ such that the horizontally polarized component of the field oscillates from +1 to -1 according to $\cos(2\alpha)$, while the term $\sin(2\alpha)$ oscillates from 0 to +1 and back to 0. As a consequence, the contribution from the $\sin(2\alpha)$ component, which does not have negative amplitudes, behaves like the Fresnel zones, giving rise to a focus at $\tau_f/2$. In Fig. 1(g), we show the expected propagation, including the contribution from the $\sin(2\alpha)$ term, which is in good agreement with our experimental results shown in Fig. 1(f).

The scalings of the peak intensities of the focusing methods, considered in our Letter, with n_0 are shown in Fig. 2 by solid lines together with the experimental results depicted by the differently colored data points. The peak focal intensity increases with increasing n_0 , corresponding to a tighter focusing time τ_{n_0} , or, equivalently, to a shorter focal length. Furthermore, the optimal wave function consistently outperforms both methods relying on Fresnel zone plates. The optimal diffractive focusing gives an improvement of $\pi^2/8$ compared to PFZ, and $\pi^2/4$ for AFZ, which manifests itself in Fig. 2 by shifts of the straight lines relative to the blue line.

We conclude this discussion by emphasizing that with our PBOE we were able to achieve a better resolution in our pattern creation, allowing for a tighter focusing time τ_{n_0} with $n_0=14$, than with the SLM. This advantage is primarily due to the fact that a diffraction grating is necessary when the SLM is used to form an arbitrary wave function, which thus limits the maximum spatial frequency of the phase oscillations corresponding to the desired pattern. In addition, the SLM has limited control over both phase and spatial modulation, as prescribed by its bit depth and pixel pitch, respectively. As n_0 is increased, the number of oscillations in $\psi_0^{(\text{opt})}$ from +1 to -1 increases, thereby leading to sharper modulation features in the outer region of the display.

Summary—We have derived the optimal real-valued matter wave $\psi_0^{(\text{opt})}$ for focusing in both one and two dimensions (see Appendix D for one-dimensional case). The same form of the Schrödinger equation for matter wave and the paraxial wave equation for electromagnetic waves allows us to transfer our treatment to light. In our optical experiment, we have realized the two-dimensional optimal wave function $\psi_0^{(\text{opt})}$ using liquid crystal devices, verifying the best possible focusing properties of $\psi_0^{(\text{opt})}$ compared to diffractive focusing from Fresnel zone patterns.

The optimal diffractive patterns derived here are of great interest to many different communities where phase modulation, due to technological limitations, is not directly possible. We can also envision extending this technique to vector fields, such as spinors in both optical and matter waves, where combinations of amplitude masks and

specially polarized vector modes bring highly structured variations in focused beams [17–19]. The application of $\psi_0^{(\text{opt})}$ to these tight focusing problems remains to be explored.

Acknowledgments—Maxim A. Efremov and Felix Hufnagel contributed equally to this work. We thank P. Boegel for fruitful discussions. W. P. S. is grateful to the Hagler Institute for Advanced Study at Texas A&M University for a Faculty Fellowship, and to Texas A&M AgriLife Research for the support of this work. This project was conceived during a visit of E. K. to Ulm University made possible by *IQST*. F. H. and E. K. acknowledge the support of the Canada Research Chair (CRC) Program, NRC-uOttawa Joint Centre for Extreme Quantum Photonics (JCEP), and NSERC.

- [1] M. Born and E. Wolf, *Principles of Optics: Electromagnetic Theory of Propagation, Interference and Diffraction of Light* (Cambridge University Press, New York, 1999).
- [2] M. Khorasaninejad and F. Capasso, Metalenses: Versatile multifunctional photonic components, Science 358, eaam8100 (2017).
- [3] A. Arbabi and A. Faraon, Advances in optical metalenses, Nat. Photonics **17**, 16 (2023).
- [4] R. Menon and B. Sensale-Rodriguez, Inconsistencies of metalens performance and comparison with conventional diffractive optics, Nat. Photonics 17, 923 (2023).
- [5] W. T. Chen, A. Y. Zhu, V. Sanjeev, M. Khorasaninejad, Z. Shi, E. Lee, and F. Capasso, A broadband achromatic metalens for focusing and imaging in the visible, Nat. Nanotechnol. 13, 220 (2018).
- [6] S. Banerji, M. Meem, A. Majumder, F. G. Vasquez, B. Sensale-Rodriguez, and R. Menon, Imaging with flat optics: Metalenses or diffractive lenses?, Optica 6, 805 (2019).
- [7] M. A. Cirone, K. Rzążewski, W. P. Schleich, F. Straub, and J. A. Wheeler, Quantum anticentrifugal force, Phys. Rev. A 65, 022101 (2001).
- [8] I. Białynicki-Birula, M. A. Cirone, J. P. Dahl, M. Fedorov, and W. P. Schleich, In- and outbound spreading

- of a free-particle s-wave, Phys. Rev. Lett. **89**, 060404 (2002)
- [9] W. B. Case, E. Sadurni, and W. P. Schleich, A diffractive mechanism of focusing, Opt. Express **20**, 27253 (2012).
- [10] D. Weisman, S. Fu, M. Gonçalves, L. Shemer, J. Zhou, W. P. Schleich, and A. Arie, Diffractive focusing of waves in time and in space, Phys. Rev. Lett. 118, 154301 (2017).
- [11] D. Weisman, C. M. Carmesin, G. G. Rozenman, M. A. Efremov, L. Shemer, W. P. Schleich, and A. Arie, Diffractive guiding of waves by a periodic array of slits, Phys. Rev. Lett. **127**, 014303 (2021).
- [12] P. Boegel, M. Meister, J.-N. Siemß, N. Gaaloul, M. A. Efremov, and W. P. Schleich, Diffractive focusing of a uniform Bose–Einstein condensate, J. Phys. B 54, 185301 (2021).
- [13] D. Attwood, Soft X-Rays and Extreme Ultraviolet Radiation: Principles and Applications (Cambridge University Press, Cambridge, England, 1999).
- [14] M. Abramowitz and I. A. Stegun, Handbook of Mathematical Functions with Formulas, Graphs, and Mathematical Tables (US Government Printing Office, 1968), Vol. 55.
- [15] H. Larocque, J. Gagnon-Bischoff, F. Bouchard, R. Fickler, J. Upham, R. W. Boyd, and E. Karimi, Arbitrary optical wavefront shaping via spin-to-orbit coupling, J. Opt. 18, 124002 (2016).
- [16] E. Bolduc, N. Bent, E. Santamato, E. Karimi, and R. W. Boyd, Exact solution to simultaneous intensity and phase encryption with a single phase-only hologram, Opt. Lett. **38**, 3546 (2013).
- [17] R. Dorn, S. Quabis, and G. Leuchs, Sharper focus for a radially polarized light beam, Phys. Rev. Lett. 91, 233901 (2003)
- [18] H. Wang, L. Shi, B. Lukyanchuk, C. Sheppard, and C. T. Chong, Creation of a needle of longitudinally polarized light in vacuum using binary optics, Nat. Photonics 2, 501 (2008).
- [19] E. Karimi, B. Piccirillo, L. Marrucci, and E. Santamato, Improved focusing with Hypergeometric-Gaussian type-II optical modes, Opt. Express 16, 21069 (2008).

 $B \equiv \int_0^1 v \, \mathrm{d}v \, \sin\left(\frac{v^2}{2\tau_{\rm E}}\right) \psi_0(v)$

are functions solely of $\tau_{\rm f}$.

(A3), and obtain the system

(A3)

End Matter

Appendix A: Optimal state in two dimensions—To obtain the analytical solution of the integral equation (5) of the Letter, we cast it in the form

$$\psi_0(u) = \frac{1}{2\pi\tau_r^2\lambda} \left[A \cos\left(\frac{u^2}{2\tau_f}\right) + B \sin\left(\frac{u^2}{2\tau_f}\right) \right], \quad (A1)$$

where

$$A \equiv \int_0^1 v \, \mathrm{d}v \, \cos\left(\frac{v^2}{2\tau_\mathrm{f}}\right) \psi_0(v) \tag{A2}$$

$$A \equiv \int_0^{\infty} v \, \mathrm{d}v \, \cos\left(\frac{1}{2\tau_{\mathrm{f}}}\right) \psi_0(v) \tag{}$$

$$\left[\lambda - \frac{1 + \tau_{\rm f} \sin(1/\tau_{\rm f})}{8\pi\tau_{\rm f}^2}\right] A - \frac{\sin^2[1/(2\tau_{\rm f})]}{4\pi\tau_{\rm f}} B = 0 \qquad (A4)$$

Next, we insert ψ_0 given by Eq. (A1) into Eqs. (A2) and

$$-\frac{\sin^2[1/(2\tau_{\rm f})]}{4\pi\tau_{\rm f}}A + \left[\lambda - \frac{1 - \tau_{\rm f}\sin(1/\tau_{\rm f})}{8\pi\tau_{\rm f}^2}\right]B = 0 \quad (A5)$$

and

of algebraic equations for A and B, which has nontrivial solutions, only when its determinant is zero, that is

$$\left(\lambda - \frac{1}{8\pi\tau_{\rm f}^2}\right)^2 - \left(\frac{\sin[1/(2\tau_{\rm f})]}{4\pi\tau_{\rm f}}\right)^2 = 0. \tag{A6}$$

This elementary quadratic equation has the two solutions

$$\lambda_{\pm} = \frac{1}{8\pi\tau_{\rm f}^2} \left[1 \pm 2\tau_{\rm f} \left| \sin\left(\frac{1}{2\tau_{\rm f}}\right) \right| \right]. \tag{A7}$$

By inserting the maximal eigenvalue λ_+ into Eq. (A4), we find the relation between A and B, and thus the normalized optimal initial wave function $\psi_0^{(\text{opt})}$ given by Eq. (7) of the Letter.

Appendix B: Maximal intensity of Fresnel zones—For a given value of τ_f the radii

$$\rho_n \equiv \sqrt{2\pi\tau_{\rm f}n} \tag{B1}$$

of the Fresnel zones, with $n=1,2,3,...,n_0$, extend to the maximum number n_0 of zones fitting within the circular aperture $0 \le \rho \le 1$ [1]. Therefore, the initial wave functions $\psi_0^{(AFZ)}$ and $\psi_0^{(PFZ)}$ for the amplitude and phase Fresnel zone patterns read

$$\psi_0^{(\text{AFZ})}(\rho) = N_1 \bigg[\mathbb{U}(\rho; 0, \rho_1) + \sum_{n=1}^{\infty} \mathbb{U}(\rho; \rho_{2n}, \rho_{2n+1}) \bigg] \quad (\text{B2})$$

and

$$\psi_0^{(PFZ)}(\rho) = \frac{1}{\sqrt{\pi}} \left[\mathbb{U}(\rho; 0, \rho_1) + \sum_{n=1}^{\infty} (-1)^n \mathbb{U}(\rho; \rho_n, \rho_{n+1}) \right]$$
(B3)

with $\mathbb{U}(\rho; a, b) \equiv \Theta(b - \rho) - \Theta(a - \rho)$ and a < b. Here, $\Theta(\rho)$ denotes the Heaviside function and N_1 is a normalization factor depending on τ_f .

To derive an analytical formula for the maximal intensity, we choose the focusing times $\tau_{\rm f} \equiv \tau_{n_0} \equiv 1/(2\pi n_0)$. In this case, Eq. (B1) reduces to $\rho_n = \sqrt{n/n_0}$, and the normalization condition

$$\pi N_1^2 [\rho_1^2 + (\rho_3^2 - \rho_2^2) + (\rho_5^2 - \rho_4^2) + \ldots] = 1 \quad \text{ (B4)}$$

for $\psi_0^{(AFZ)}$, Eq. (B2), defines the factor

$$N_1 \equiv \sqrt{\frac{2}{\pi}} \begin{cases} \sqrt{\frac{n_0}{n_0 + 1}}, & n_0 = 1, 3, 5, \dots \\ 1, & n_0 = 2, 4, 6, \dots \end{cases}$$
(B5)

as a function of n_0 .

Next, we insert the initial profile $\psi_0^{(AFZ)}$ given by Eq. (B2) into Eq. (3) of the Letter, and obtain the expression

$$\begin{split} I_{\text{max}}^{(\text{AFZ})}(\tau_{n_0}) &= \frac{1}{\tau_{n_0}^2} \bigg| \int_0^1 u \mathrm{d}u \, \exp \left(\mathrm{i} \frac{u^2}{2\tau_{n_0}} \right) \psi_0^{(\text{AFZ})}(u) \bigg|^2 \\ &= N_1^2 \bigg| \exp \left[\mathrm{i} \frac{\rho_1^2}{2\tau_{n_0}} \right] - 1 + \exp \left[\mathrm{i} \frac{\rho_3^2}{2\tau_{n_0}} \right] \\ &- \exp \left[\mathrm{i} \frac{\rho_2^2}{2\tau_{n_0}} \right] + \ldots \bigg|^2, \end{split}$$

that is

$$I_{\text{max}}^{(\text{AFZ})}(\tau_{n_0}) = N_1^2 \begin{cases} (n_0 + 1)^2, & n_0 = 1, 3, 5, \dots \\ n_0^2, & n_0 = 2, 4, 6, \dots, \end{cases}$$
 (B6)

where we have used the fact that $\rho_n^2/(2\tau_{n_0}) = n\pi$.

As a result, Eq. (B6) combined with Eq. (B5) gives rise to the maximum intensity $I_{\rm max}^{\rm (AFZ)}(\tau_{n_0})$, Eq. (10) of the Letter, produced by the amplitude Fresnel zones. Analogously, we derive the corresponding maximum intensity $I_{\rm max}^{\rm (PFZ)}(\tau_{n_0})$, Eq. (11) of the Letter, for the Fresnel phase zones.

Appendix C: Pancharatnam-Berry optical element— Our device consists of a patterned layer of birefringent nematic liquid crystals whose orientation locally determines that of the medium's optical axis. This feature causes the element to have the action

$$\hat{\mathcal{U}}_{q} \cdot \begin{pmatrix} \mathbf{e}_{H} \\ \mathbf{e}_{V} \end{pmatrix} = \cos \begin{pmatrix} \frac{\delta}{2} \end{pmatrix} \begin{pmatrix} \mathbf{e}_{H} \\ \mathbf{e}_{V} \end{pmatrix} \\
+ i \sin \begin{pmatrix} \frac{\delta}{2} \end{pmatrix} \begin{pmatrix} \cos [2\alpha(x,y)] & \sin [2\alpha(x,y)] \\ \sin [2\alpha(x,y)] & -\cos [2\alpha(x,y)] \end{pmatrix} \\
\times \begin{pmatrix} \mathbf{e}_{H} \\ \mathbf{e}_{V} \end{pmatrix} \tag{C1}$$

on the horizontal \mathbf{e}_{H} and vertical \mathbf{e}_{V} polarization components of an optical beam. Here δ is the optical retardation of the liquid crystal molecules and $\alpha \equiv \alpha(x,y)$ is the device's spatially dependent liquid crystal axis orientation expressed in terms of the transverse Cartesian coordinates x and y.

When the device is perfectly tuned, that is for $\delta=\pi$, and followed by a *horizontally oriented polarizer*, it can effectively be used to mask the amplitude profile of incoming *horizontally polarized light* by a factor of $\cos\left[2\alpha(x,y)\right]$. This procedure was employed to generate our real-valued optimal initial wave function $\psi_0^{(\text{opt})}\equiv\psi_0^{(\text{opt})}(x,y)$ by means of a device defined by an optical axis of $\alpha(x,y)=(1/2)\arccos\left[\psi_0^{(\text{opt})}(x,y)/\psi_{\text{max}}^{(\text{opt})}\right]$, where

 $\psi_{\max}^{(\text{opt})}$ is the maximum value of the optimal initial wave function.

Appendix D: Optimal state in one dimension—In this section we determine the optimal initial real-valued and normalized wave function $\varphi_0 \equiv \varphi_0(x)$ that maximizes the intensity $|\varphi(0)|^2$ of the field at x=0, at the focusing time $t_{\rm f}$.

In this case we use the one-dimensional Green's function

$$G^{(1)}(\xi,\tau|\xi',0) = \frac{1}{\sqrt{2\pi i \tau}} \exp\left[i\frac{(\xi-\xi')^2}{2\tau}\right] \qquad (D1)$$

for the time-dependent one-dimensional Schrödinger equation of a free particle. Here, $\xi \equiv x/L$ and $\tau \equiv \hbar t/(ML^2)$ are the dimensionless position and time, respectively, and M and L denote the mass of the particle and the slit width.

We again apply the method of the Lagrange multipliers and arrive at the eigenvalue problem

$$\frac{1}{2\pi\tau_{\rm f}} \int_{-1}^{1} \mathrm{d}\xi' \, \cos\left(\frac{\xi^2 - \xi'^2}{2\tau_{\rm f}}\right) \varphi_0(\xi') = \mu \varphi_0(\xi) \quad \text{(D2)}$$

for the optimal initial wave function φ_0 with the eigenvalue μ , that determines the maximum intensity achieved at τ_f . Here, we have assumed that $\varphi_0(\xi) = 0$ for $|\xi| > 1$.

Since we are interested in the maximum of the intensity, we solve the integral equation (D2) only for the largest eigenvalue $\mu_{+}(\tau_{\rm f})$. As a result, for a given $\tau_{\rm f}$, we find the

optimal initial wave function

$$\varphi_0^{(\text{opt})}(\xi) = \sqrt{\frac{1+r}{4\pi\tau_f\mu_+}}\cos\left(\frac{\xi^2}{2\tau_f}\right) + \sqrt{\frac{1-r}{4\pi\tau_f\mu_+}}\sin\left(\frac{\xi^2}{2\tau_f}\right)$$
(D3)

for $|\xi| \le 1$, with $\varphi_0^{(\text{opt})}(\xi) = 0$ for $|\xi| > 1$, and the corresponding maximal eigenvalue

$$\mu_{+}(\tau_{\rm f}) = I_{\rm max}^{(1{\rm D})}(\tau_{\rm f}) = \mathcal{I}\left[\sqrt{2/(\pi\tau_{\rm f})}\right].$$
 (D4)

Here we have expressed the intensity

$$\mathcal{I}(z) \equiv \frac{1}{4} \left\{ z^2 + z \sqrt{[C(z)]^2 + [S(z)]^2} \right\}$$

and the parameter

$$r(\tau_{\rm f}) \equiv \frac{C\left[\sqrt{2/(\pi\tau_{\rm f})}\right]}{\sqrt{\left\{C\left[\sqrt{2/(\pi\tau_{\rm f})}\right]\right\}^2 + \left\{S\left[\sqrt{2/(\pi\tau_{\rm f})}\right]\right\}^2}}$$
(D5)

in terms of the Fresnel integrals C and S [14].